Acta Astronautica 211 (2023) 702–715

Contents lists available at ScienceDirect

Acta Astronautica

journal homepage: www.elsevier.com/locate/actaastro

Research paper

A water vapour fuelled Hall Effect Thruster: Characterization and comparison with oxygen

J.M. Tejeda *, A. Knoll

Space Propulsion Laboratory, Department of Aeronautics, Imperial College London, Exhibition Road, South Kensington, London, SW7 2BX, United Kingdom

ARTICLE INFO

Keywords:
Hall Effect Thrusters
Electric propulsion
Water vapour
Water electrolysis
Water condensation
Water feed system
Reactive model

ABSTRACT

A Hall Effect Thruster propelled by water vapour is investigated at the Imperial Plasma Propulsion Laboratory. For that purpose, a water vapour feed system is designed, optimized and tested, with the major objective of keeping water in vapour state at all times. This system primarily consists of a mass flow controller, a flow restrictor, and a heating and pressure monitor system capable of identifying under which conditions water condensation occurs. A hanging pendulum thrust balance is used to measure the thrust on the power range of P_d = 600–1600 W. Different magnetic field strengths and mass flows are investigated to determine the conditions in which the highest efficiency can be achieved. Then, a comparison between water vapour and oxygen (intended to be the propellant of a water electrolysis Hall Effect Thruster) is included. The results show that oxygen is approximately 20% more efficient than water vapour under the same operating conditions. Overall, the highest thrust measurement recorded with water vapour was 20.0 ± 0.2 mN; with a specific impulse of 2039 ± 20 s and an anode efficiency of 12.5 ± 0.3% at the largest discharge power of investigation (P_d = 1600 ± 1 W).

1. Introduction

Since the first space programmes in the 1960s, Electric Propulsion (EP) technologies have been widely used to propel spacecraft in space [1]. Not surprisingly, the extensive international research efforts in this technology have resulted in very sophisticated and efficient methods for moving any kind of space vehicle. From high power Gridded Ion Engines (GIE) and Hall Effect Thrusters (HETs) to miniaturized electrospray devices, the EP market has revolutionized the space sector and influenced the global population. Within this variety of technologies, HETs are strategically placed in Geostationary Orbits (GEOs) and mainly selected for telecommunications missions where the EP subsystem is in charge of different operations, such as North-South Station Keeping (NSSK), East West Station Keeping (EWSK) or momentum management [2]. In fact, 70% of space propulsion systems for GEOs mission use HETs [3].

Water propulsion stands out as a promising choice for EP devices and specially HETs, featuring several traits which can make them competitive compared to the state of the art HETs (which use xenon as a propellant in the majority of the cases). Some of them are their low price, non-toxicity, ease of handling and the presence in the vicinities of the Solar System, which can unlock future In-Situ Resource Utilization (ISRU) missions [4]. As an example, the Moon could be used as a fuelling station by extracting water from its surface. which is then used as a propellant to visit other planets. This strategy will alleviate the high cost of transporting propellant from Earth, enhancing the mission objectives. These future asteroid, rendezvous or planetary exploration missions will require high specific impulse (I_{sp}) thrusters, which is something commonly granted by utilizing lightweight propellants (like water). At the same time, the synergies of water with other subsystems, such as thermal management, life support systems in manned missions or inertia distribution enable hybrid architectures which no other propellant can [5]. Even more importantly: water is environmentally friendly, and its use does not compromise the Earth, favouring the sustainability of the space sector.

On the contrary, although xenon is sometimes referred to as a green propellant when compared to hydrazine, the high environmental carbon footprint of the processes used to generate it makes it far from a green propellant. This is mainly due to the low concentration of xenon on the Earth which makes its extraction and purification a very difficult and energy intensive process [6]. Previous studies on the same topic have calculated that just the extraction of xenon from a Primary Krypton Concentrate (a mix obtained after some other processes of air purification) can need up to 4353 kWhs per each kg of xenon produced [5,7]. An analysis based on greenhouse gas reports estimates that producing this amount generates just over 1000 kg of CO_2 [8]. Its

* Corresponding author.
E-mail address: jesus.munoz.tejeda@imperial.ac.uk (J.M. Tejeda).

https://doi.org/10.1016/j.actaastro.2023.06.046
Received 27 March 2023; Received in revised form 19 April 2023; Accepted 26 June 2023
Available online 4 July 2023

high price and associated volatility [9,10] also create a strong economic barrier for small companies which want to play a role in the electric propulsion field [11].

Looking to tackle these problems and make use of its benefits, the prospects of water as an alternative propellant in the community of EP, (and more specifically, in HETs) are encouraging for medium-term space mission. Within water propulsion HETs, two different alternatives are conceptualized: water vapour and water electrolysis.

1.1. Water electrolysis (oxygen and hydrogen)

In water electrolysis HETs propulsion, it is proposed that an electrolyzer onboard of the spacecraft could separate water into oxygen (propellant used for the thruster) and hydrogen (for the cathode). The exploration of the thruster working with oxygen has been the focus of several years of experimentation at the Imperial College London Plasma Propulsion Laboratory (IPPL). There, several systematic studies have explored the computational [12] and experimental performance of a Water Electrolysis Hall Effect Thruster under diverse magnetic field configurations, mass flows and discharge chamber axial lengths [11, 13,14]. All the lessons learnt from these experiments are considered when testing under the new conditions presented in this paper, using water vapour.

1.2. Water vapour

In water vapour HETs, direct water in the gaseous phase would be fed into the thruster. Because of that, water vapour technologies do not need an electrolyzer on board of the spacecraft, which signifies less mass, volume and complexity penalties. In the literature, water vapour has been investigated for other types of EP systems, such as Helicon Thrusters [15], Electrodeless ECR thrusters [16,17] and Ion Thrusters [18,19]; although no profound study has yet been carried out in HETs.

Using this research, it is possible to bring deeper insights into water vapour HETs technology and to compare them against water electrolysis HETs, using the lessons learnt over the last years of experimentation working with these technologies.

Section 2 gives an overview of the hardware used for the experimental investigation: facilities, thruster, thrust balance (see Fig. 1), water feed system and water condensation control system. Section 3 compares the physical properties of water vapour and oxygen, considering their respective reactive model and their collisional cross-section. Section 4 shows the results of the water vapour tests (mass flow dependence, magnetic field dependence and power dependence compared to oxygen). In Section 5, a trade-off analysis between water vapour and water electrolysis is performed, based on the lessons learnt from the experimentation and previous analyses. Making use of all of this, it is possible to study which technology might be more suitable depending on the space mission requirements. Lastly, Section 6 gives the final remarks, discussions and future work of this technology.

2. Materials and methods

2.1. Testing facilities

The experimental campaigns were carried out at the Boltzmann vacuum chamber facilities of the IPPL. Three vacuum stages allowed to have vacuum levels in the order of 10^{-5} mbar during operation, conditions which are maintained throughout all the tests. More information about these vacuum pumps is available in previous work [14]). Appendix shows the schematic setup of these systems in the laboratory.

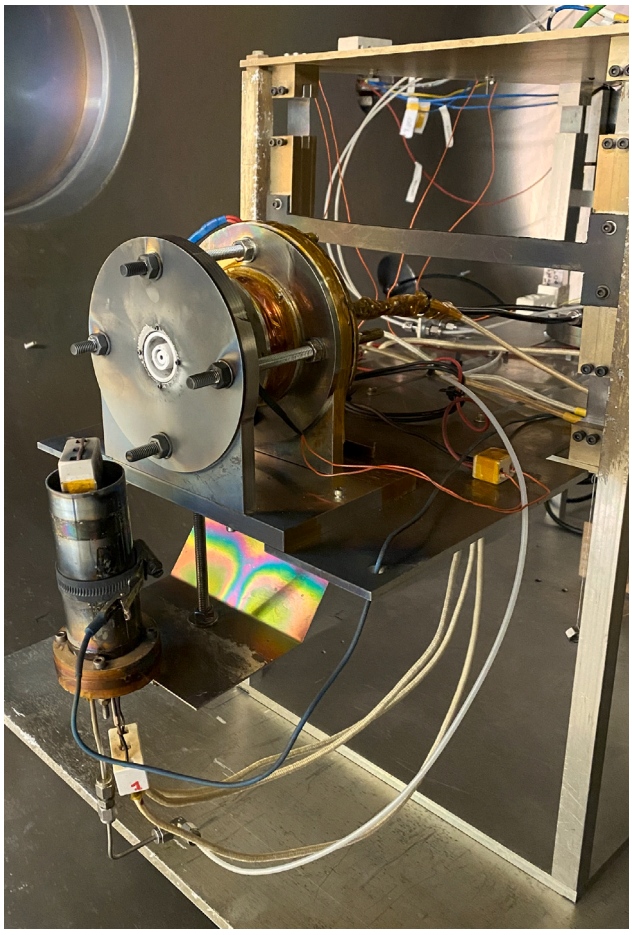

Fig. 1. The laboratory HET and cathode mounted in the thrust balance at IPPL vacuum chamber facilities.

2.2. Laboratory HET

The HET used for the experimentation is shown in Fig. 1. In related investigations, this HET is known as the Water Electrolysis Hall Effect Thruster (the *WET-HET*), making reference to a HET optimized to work with molecular propellants such as oxygen (see Section 1.1) [11,13,14]. The mechanical and thermal properties of the thruster can be found in previous work of A. Schwertheim [20]. In this paper, this thruster is used to conduct water vapour experiments. The idea is to replicate the same setup as with water electrolysis testing, such that a fair comparison between oxygen and water vapour can be conducted. To start with, previous research on this thruster experimentally demonstrated that, for molecular propellants, longer channels do not improve the performance of the thruster [14]. The best performing case was found with a channel length of around 13 mm, and therefore this geometrical parameter is fixed throughout all testing campaigns. These studies also found the most suitable ceramic wall material (a Boron Nitride Silicon compound $BNSiO_2$ Grade M26), due to its low secondary electron emission (SEE) and hydrophobic characteristics, with help to absorb moisture from water vapour (either from oxygen and hydrogen coming from the water electrolyzer itself, or for the water vapour feed in this case) [14]. The anode material is made of stainless steel, as tungsten, despite its good thermal properties, was found to develop an oxidation layer when in contact with the oxygen plasma, preventing long-term testing [14]. With this fixed geometrical configuration, it is possible to determine the quantity of water vapor particles injected per second per anode area for two distinct mass flow rates (0.7 mg/s and 1.0 mg/s, as presented in Table 1 for a comprehensive compilation of the thruster's

Table 1
Experimental configuration of the HET used during water vapour testing.

Variable	Value
Channel width, [mm]	5
Channel outer diameter, [mm]	25
Channel length, [mm]	13
Magnetic topology	Fig. 2
Mass flow rate [mg/s]	0.7–1.0
Particles injected per second per area [# / (s mm^2)]	7.4×10^{16} – 1.1×10^{17}
Power Range [W]	600–1600
Channel walls	$BNSiO_2$ (Grade M26)
Anode material	Stainless Steel

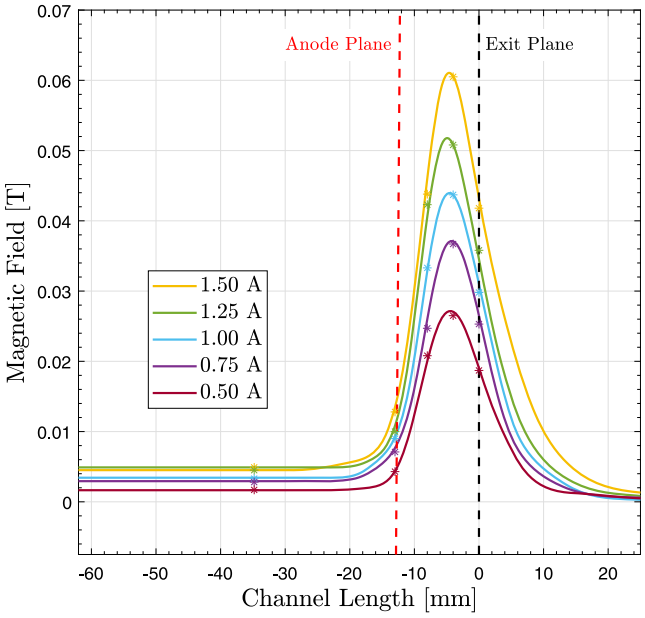

Fig. 2. Magnetic field topology of the laboratory HET as a function of the current driven throughout the electromagnets. The dots represent experimental measurements.

mechanical characteristics). Comparatively, these values are approximately sevenfold greater than those encountered when utilizing this HET with xenon, operating at the same mass flow rate and geometrical configuration.

Moreover, in the case of the *WET-HET*, the number of particles injected per second per anode area is significantly higher than the quantities employed, for instance, in the geometrical configuration of the *SPT-100* when running on xenon. By considering the two mass flow rate limits of 3.4 mg/s and 6.6 mg/s [21,22], it becomes evident that approximately ten to twenty times more particles are introduced per second per anode area in the case of the *WET-HET*. This serves as tangible evidence of the inherent inefficiencies associated with the utilization of alternative propellants in HETs.

Under these conditions, several studies over different magnetic field strength, propellant mass flow and power dependence are carried out. The magnetic field is generated by means of electromagnets. Fig. 2 shows the relationship between the current flowing through the coils and the magnetic field strength. At the maximum current (1.5 A) the power used by the electrocoils is $P_m = 27$ W.

The location of the anode plane with respect to the exit plane (13 mm) is also represented. This plot is obtained from Finite Element Method Magnetics simulations [20] and corrected using experimental data (represented by dots on Fig. 2).

Table 2
Description of the water feed system elements used to test the HET with water vapour.

A	H_20 bottle container
B	Manual Valve (to control water flow)
C	Manual Valve (to evacuate bubbles)
D	Liquid Mass Flow Controller (Bronkhorst L13V12)
E	Flow restrictor (liquid to vapour water transition)
F	Pressure transducer
G	Heating system
H	Transparent feedline (to check condensation)
I	Manual Valves set

2.3. Thrust balance

The thrust measurements were collected using a hanging pendulum thrust balance. This device has been widely used during previous experimental campaigns [11,13,14] and validated in different laboratories. A detailed description of the functionality of the trust balance and its principles for acquiring thrust measurements can be found in [23]. Fig. 1 shows the thruster mounted on the thrust balance prior to testing.

2.4. Laboratory cathode

For the cathode, a plasma filament bridge neutralizer [24] was used (see [14] for more information about its working principle). The edge of the cathode is located approximately 42 mm from the exit plane, and the centreline at 60 mm (see Fig. 1); consistent with previous campaigns [11,13,14]). For both, water electrolysis and water vapour, there are technical challenges in the operation of hollow cathodes with reactive gases, due to the poisoning of the Lanthanum Hexaboride (LaB_6) insert [25]. Diverse studies show that, for water electrolysis, hydrogen counteracts poisoning [26,27], although its practical feasibility needs to be further explored. However, in water-vapour propulsion, the most suitable propellant selection for the hollow cathode remains an open question.

One possible approach would be the use of a microwave cathode, where the use of alternative propellants such as water vapour does not compromise the integrity of the same. The use of a microwave water vapour cathode in ion thrusters has been already explored and experimentally tested by T. Motoki et al. [28]. In this paper, the main focus resides on the characterization and feasibility evaluation of the thruster, and deeper cathode compatibility studies are set as the next phases of the investigation. The propellant used for the experiments is Krypton, with mass flow rates between 5–15 sccm. Experimentally, it is tested that the cathode mass flow rate had no significant impact on the thrust measurements.

2.5. Water vapour feed system

Table 2 and Fig. 3 show the components of the water vapour feed system. The actual representation during testing is displayed in Fig. 4. Lastly, Fig. 5 shows the HET with the water vapour feed system in an open-out configuration (FlatSat). A full depiction of the experimental setup, including the rest of the hardware and electronics of the experiment, is included in Appendix.

The starting point of the water vapour feed system is a water tank [A] where distilled water is stored at atmospheric pressure. The tank is arranged so that it does not leak water but allows air to enter. By doing so, the air pushes the water down and helps the water travel through the rest of the line. A manual valve [B] controls the flow of water from the container. Further down the line, there is another valve [C] that is open to evacuate trapped bubbles in the feedline. Once the feedline between B and C is free of bubbles, the valve [C] is closed. Next to it, there is a liquid mass flow controller [D] (model Bronkhorst L13V12). The reason behind selecting a liquid mass flow controller instead of

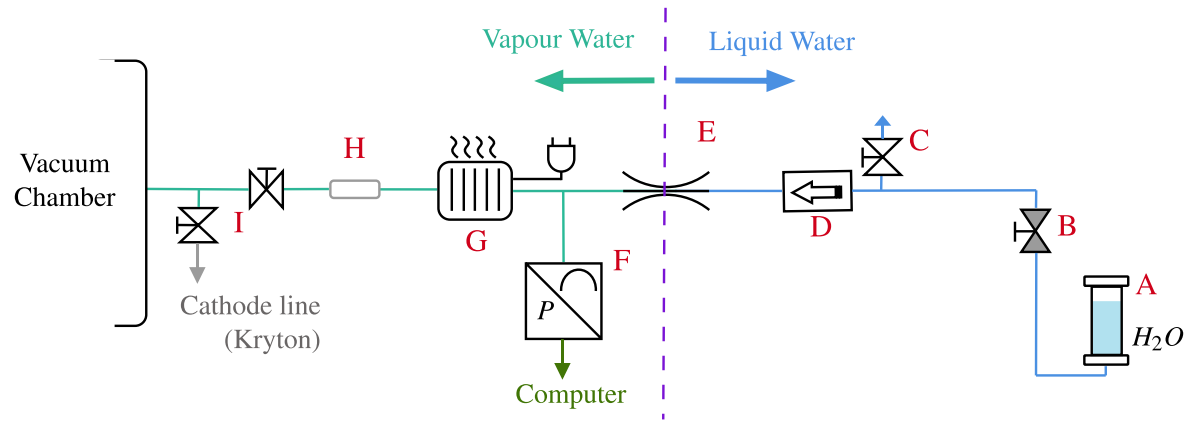

Fig. 3. Diagram of the water feed system used for the HET electric propulsion testing at the IPPL facilities.

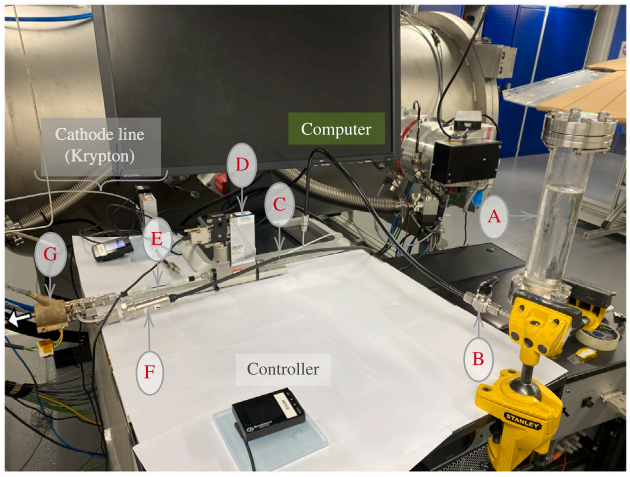

Fig. 4. Water feed system disposition during testing at IPPL facilities.

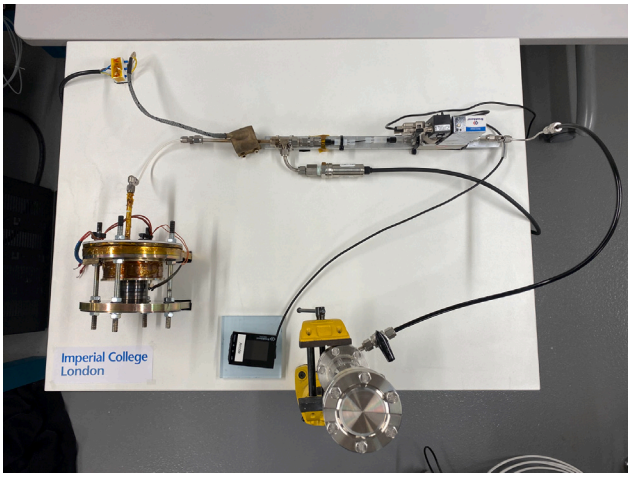

Fig. 5. Water feed system and HET in Opened-out 'FlatSat' configuration.

a gas flow controller is to have a higher precision of the flow that is coming to the thruster. Notice that up to this point (from [A] to [D]), the water is still in the liquid phase. The phase change occurs not until the flow restrictor [E].

At this point (just before the flow restrictor), it is recommended to add a particle filter, such that the line does not get clogged at any point during the operation. The flow restrictor itself consists of a polyetheretherketone (PEEK) capillary tube with a very thin orifice (100 μm) and an outer diameter of 1/16"; together with a set of perfluoroalkoxy (PFA) fittings, 1/4-28 unions and ethylene tetrafluoroethylene (ETFE) flangeless ferrules. This set ensures a compatible fit between the capillary tube and a standard Swagenlok 1/8" tube. This hardware was acquired from *Darwin Microfluidics* [29]. The phase transition from liquid to water vapour comes as follows: at the entrance of the flow restrictor, the water sees a very high resistance when trying to flow over the thin orifice. Notice that the smaller the orifice of the tube, the higher the fluidic resistance. After crossing the 100 μ m tube, the water, still in the liquid phase, suddenly expands back into the feedline tube (1/8"). This sudden expansion causes a subsequent phase change. The pressure at this point is controlled by a pressure transducer [F] which is monitored by computer software. As it will be explained in Section 2.6, this is the part of the line with the highest pressure and consequently the one where water condensation is more likely to occur, hence the placement of the pressure transducer there. To maintain the water gas, a heating system warms the feedline [G]. A transparent tube section [H] sits after the heating line to visually check if water condensation has happened. Finally, a strategic set of valves [I] is placed to allow the possibility of using krypton (gas used for the cathode) to trigger the thruster plasma discharge before swapping to water vapour. Although not necessary in all cases, this methodology prevents an initial sparking of the thruster due to the inherent difficulties of ignition with water vapour compared to krypton. Other ignition strategies can be found in previous work [14].

2.6. Water condensation control system

The water condensation control system consists of a pressure [F] and temperature [G] monitor system, together with a transparent feedline tube [H] to visually inspect if water condensation has occurred. The readings of the pressure transducer over time for two different mass flows (1 mg/s and 3 mg/s) are displayed in Fig. 6. Notice that, during these readings, the heating system is activated, which warms the feedline and helps to mitigate water condensation. The theoretical values for water condensation at a certain pressure and temperature (300K, 302 K and 304 K) are also displayed. These values are obtained using the open source programme *CoolProp* [30]. For 1 mg/s of water vapour mass flow, the readings of the pressure transducer stay constant between 20 to 25 mbar, way below any water condensation for temperatures above 300 K. However, for mass flows of 3 mg/s, peaks on the pressure reading appear after some time of operation. These peaks correspond to sudden pressure losses resulting from condensation of water on the line. Consequently, mass flows of 3 mg/s or higher end up with water condensation and cannot be used to test the thruster with the current set-up. Mass flows of 2 mg/s or below are suitable

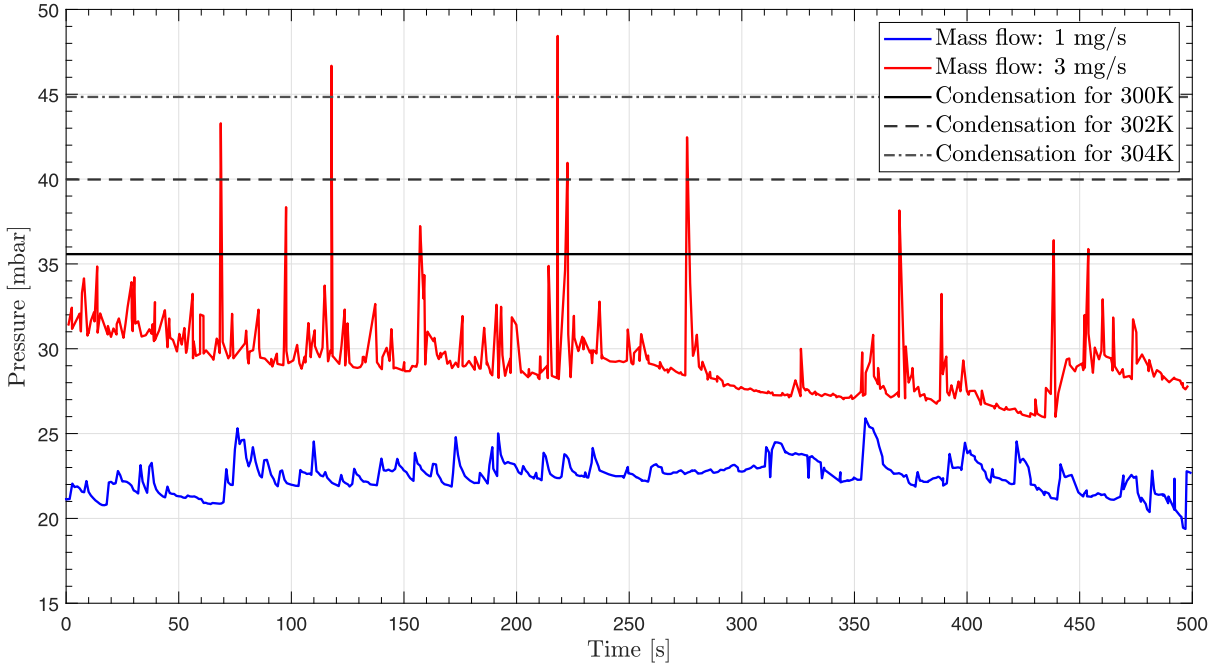

Fig. 6. Water pressure in the feedline just after the flow restrictor, for various mass flow rates and a heating system activated. The experimental data is compared with the theoretical condensation pressures for water condensation at 300 K, 302 K and 300 K.

for use because no condensation was detected during operation. This limitation in mass flow does not have an impact on the investigation, as the nominal operation of the thruster investigated (the *WET-HET*) is 1 mg/s [11].

The results of this setup came after several iterations of the feedline, so minimum pressure losses arose during operation. In fact, from the first tests, condensation was spotted at 1 mg/s and below; therefore the feedline design needed to be changed. The feedline optimization was based on the Darcy–Weisbach equation, commonly used to calculate pressure losses in pipes [31]. Note that, throughout this text, when referring to the path from the flow restrictor to the chamber (from right to left in Fig. 7), the pipelines are referred to create "pressure losses". If the reference frame is inverted, now from the chamber to the flow restrictor (from left to right in Fig. 7), the feedline introduces "pressure surges" or "a pressure rise" instead. In any case, the main objective is to lessen the pressure at the flow restrictor (point of the feedline with the highest pressure, see Fig. 7) to ensure that water condensation does not occur during the tests.

For a laminar flow, the Darcy–Weisbach equation can be rewritten in terms of known quantities and expressed as [31–33]:

$$\Delta p = L\frac{128\mu Q}{\pi D_c^4} \tag{1}$$

There, Δp represents the pressure loss in the pipe, L is the length of the pipe, μ is the dynamic viscosity of the water vapour, Q is the volumetric mass flow rate (value derived from the mass flow rate of the propellant) and D_c is the diameter of the pipe through which the water travels. Eq. (1) concludes that, given a mass flow rate, it is possible to reduce the pressure losses by using a shorter length of the pipes (decrease L) and/or by using a thicker pipeline diameter (increase D_c). As the term D_c is a fourth order term, increasing the pipe diameter has a much greater impact on the pressure than reducing the feedline, although the latest is also important to minimize as much as possible the pressure losses.

In the latest iteration of the feedline, the pipe diameter was changed from 1/8" to 1/4" for the majority of the line (see Fig. 7), and the total feedline length was reduced from 5.0 m to 3.5 m (see Fig. 7). Only thanks to these changes, mass flows up to 2 mg/s were able to be tested

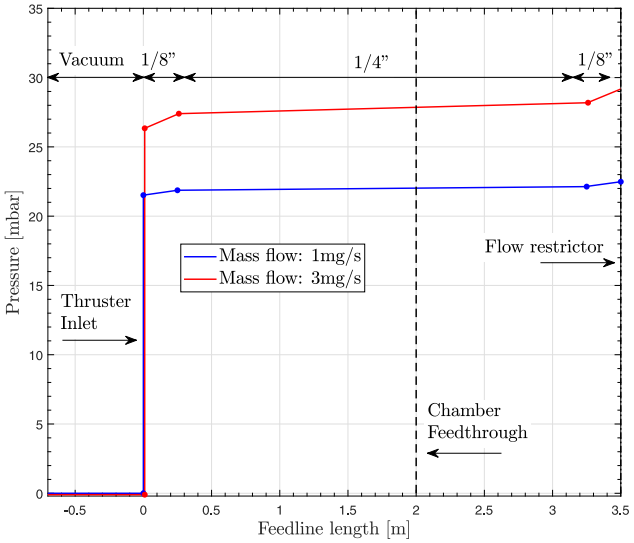

Fig. 7. Calculated pressure as a function of the feedline length. From vacuum conditions, the pressure rises at the thruster inlet and throughout the 1/4ε and 1/8ε sections due to pressure losses, until the water vapour reaches the flow restrictor (point of maximum pressure).

without creating water condensation. Notice that in Fig. 7, an average of the pressure readings is taken at the start point on the flow restrictor.

The pressure rise in the thruster inlet is calculated by setting the boundary condition of the pressure of the vacuum chamber ($\approx 10^{-5}$ mBar) at its exit. This comes from the way the propellant is introduced into the thruster: in the *WET-HET*, the propellant injection strategy consists of a 1/8" tube ending in a reservoir where the gas finds its way towards the discharge chamber by travelling through a small gap (0.5 mm) between the inner ceramic wall and the anode [13,14]. This strategy, although suitable for water electrolysis testing because the gases are naturally in vapour form, is not the most optimal for water vapour experimentation, as it develops a substantial rise in pressure

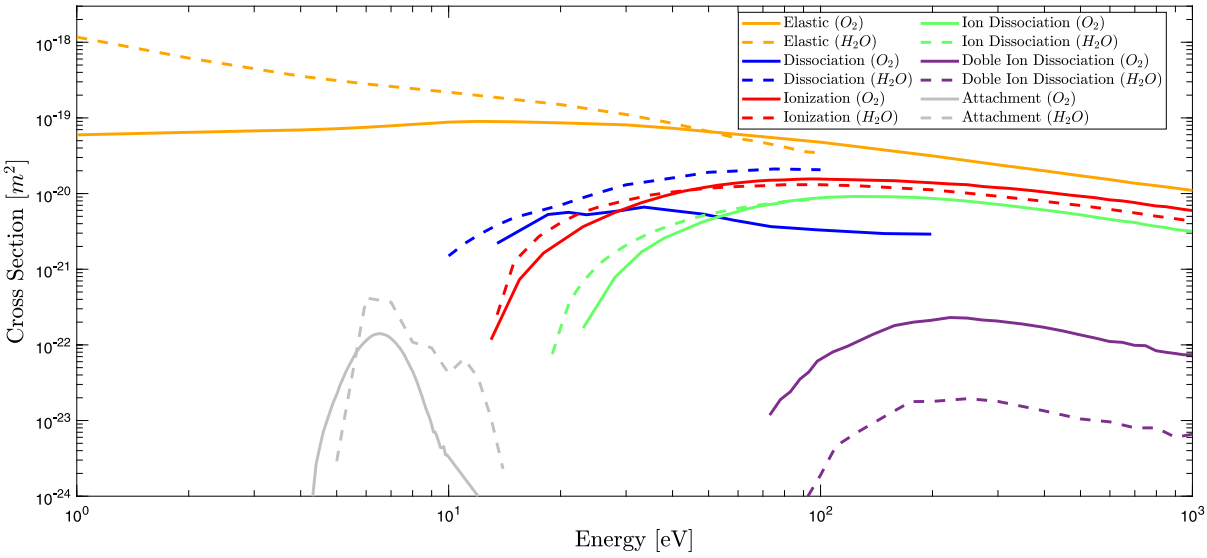

Fig. 8. Comparison of the cross-sections of water vapour and oxygen molecules, as a function of the electron energy. *Source:* Data taken from experimental results coming from diverse studies. This data is compiled and analysed by Y. Itikawa in [34,35].

(Fig. 7) which can lead to water condensation if the flow rate is too high (higher or equal to 3 mg/s in this experimentation). Other strategies in which the propellant is injected from relatively thick-diameter holes might create a lower pressure rise and allow testing under higher mass flow conditions. Even then, a pressure rise at the thruster inlet will always be present due to the small diameter of the propellant holes used to distribute the flow, typical in HETs operation. For that matter, the use of short and thick pipelines during the vapour phase is still a recommended strategy. Lastly, note that due to the incompressibility of liquid water and the small pressure drop on the liquid mass flow meter (1 mBar), liquid water is expected to be under atmospheric conditions upstream of the flow restrictor.

3. Wapor vapour and oxygen plasmas

Before proceeding to evaluate and discuss the results obtained during the experimentation, a comparison between the physical properties of water vapour and oxygen plasmas is addressed. The main purpose of this study is to broaden the understanding of their impact in the performance of a HET by looking at how different these two molecules behave with respect to each other.

To start with, the mass and Van der Waals radius of these two molecules are shown in Table 3. The mass of the particle plays an important role for two principal reasons: first, the higher the mass expelled, the higher the thrust of the HET. Second, a lighter molecule will be further accelerated, so the I_{sp} is expected to increase. Notice that the ion mass is practically the same as the mass of the neutral particle, due to the small electron mass (9.109×10^{-31} kg). From these data, it is seen that the oxygen mass is 44% greater than the water vapour so, for the same ionization conditions, a higher I_{sp} but lower thrust from the water vapour is expected. The Van der Waals radius also affects the collision rate of the particles. For the water vapour, data is directly taken from the literature [36]. For the oxygen molecule, an average is taken between the transverse (1.88 Å) and the longitudinal Van der Waals radius (1.66 Å) is taken (value equal to 1.77 Å, or 1.77×10^{-10} m) [37]. As can be seen, these values are very similar to each other.

Another important factor to consider lies on the intrinsic reactive model of these two molecules. Contrary to xenon, water vapour and oxygen molecules not only can undergo ionization, but also dissociation, double ionization and attachment events. For the thrusters' perspective, to simply ionize the plasma is the most efficient process to generate thrust. This is because the energy deposited in dissociating the particle (or ionizing it twice) is energy which does not directly contribute to the thrust. Attachment processes generate negative ions, which are accelerated inwards the channel and should be avoided. Finally, the lower the ionization potential, the higher the propellant utilization, as most of the neutral particles will be ionized and will contribute to a higher thrust.

In Fig. 8, the reactive model of water vapour is compared to the one of oxygen, using data collected once again by Y. Itikawa [34,35]. Notice that, for the water vapour model, there are different dissociation, ion dissociation and attachment events. For example, an electron collision can dissociate the water molecule obtaining OH and H, but also O and H_2. The ion dissociation events can generate ions of OH^+, O^+, H_2^+ or H^+. For attachment, negative ions of OH^-, O^- or even an attachment dissociative process that creates H^- and H can take place. The sum of these cross-sections is taken when displaying these reactions in Fig. 8. This is not the case for the oxygen molecule, where the products are unique for each type of reaction. Explicit information about every singular water vapour reaction can be found in the literature [34].

For a HET, the electron temperature varies within the channel, generally peaking at the end of the channel [38] and being a function of the discharge power, geometry and operating mass flow [1]. A general rule of thumb is to estimate the plasma temperature within the channel as one-tenth of the discharge voltage (V_d), which is a prediction that has also been observed experimentally [1,39,40]. Considering a discharge voltage of $V_d \approx 300$ V, the range of interest in the electron temperature would have a Maxwellian distribution centred at around 30 eV. On the one hand, by inspecting Fig. 8, it can be observed that, for water vapour, the dissociation cross-section is higher than the ionization cross-section (regardless of the electron energy). On the other hand, the ionization cross-section of oxygen outweighs the dissociation cross-section for electron energies above ≈15 eV. This is an indication that, for water vapour, a greater amount of energy will be used to dissociate the molecule instead of directly ionizing it, which can be a deficiency sink compared to oxygen. Attachment reactions appear for electron energies between 4–10 eV, but their cross-section is generally an order of magnitude lower than the ionization and dissociation events. A similar case occurs with double ionization processes; these reactions are mainly relevant above 100 eV, being an order of magnitude less than the ionization and dissociation events.

Table 3
Mass and Van der Waals radius of the water vapour and oxygen molecules. The ratio is obtained using the molecule of oxygen as a baseline to compare against.

	Water vapour [H_2O]	Oxygen [O_2]	Ratio
Molecular Mass [u]	18	32	56%
Van der Waals Radius [m]	1.70×10^{-10}	1.77×10^{-10}	96%

Fig. 9. Plasma plumes of the HET working with water vapour, oxygen, air (from the laboratory) and krypton.

4. Results

In order to obtain performance measurements, the HET propulsive thrust (T) is obtained from the thrust balance readings. Then, the mass flow controller and the set point of the power supply are used to obtain the mass flow rate ($\dot{m}$) and the discharge power (P_d), respectively. From them, I_{sp} and thrust efficiency (η) are calculated as follows:

$$I_{sp} = \frac{T}{\dot{m}} \tag{2}$$

$$\eta = \frac{T^2}{2\dot{m}P_d} \tag{3}$$

The uncertainty in the thrust measurements come from the thrust balance. The propagation of the error from these measurements is calculated as in previous work [23]. The thruster in operation can be seen in Fig. 9. Apart from water vapour, the thruster working with oxygen, air and krypton is shown. Further details of the electronics used for the experiment can be found in Appendix. The geometrical configuration (channel width, diameter and length) is maintained constant as shown in Table 1. Notice that, as explained in Section 2.2, this material selection and geometrical choice is taken from the outcomes of the previous research presented, which resulted in the best performing configuration for lightweight propellants, such as oxygen [14]. However, this configuration might not necessarily need to be the best one for traditional propellants such as krypton and xenon. To get a realistic view on how a traditional HET compares to the results of this thruster operating with these lightweight propellants, the *SPT-100* will be taken as a Ref. [21,22].

Lastly, note that, for consistency with the previous experimental campaigns [13,14], the performance measurements are obtained using the anode power supply in current control mode. The discharge voltage could vary 10 V between experiments due to factors not under control such as: the ceramics' walls temperature, the oxidation of the anode surface or the coupling mode of the cathode.

4.1. Mass flow dependence

In this section, the mass flow performance dependence of the HET operating with water vapour is explored. Fig. 10 shows the results obtained from the experiments. Specifically, Fig. 10(a) presents the IV curve for two different mass flow rates: 1.0 mg/s and 2.0 mg/s. Thrust to Power Ratio (TTPR) as a function of the I_{sp} is calculated in Fig. 10(b). Thrust (Fig. 10(c)), I_{sp} (Fig. 10(d)) and thrust efficiency (Fig. 10(e)) of the thruster over the mass flow range of $\dot{m} = 0.7 - 1.0$ mg/s are also shown. The discharge power at which these measurements are taken is $P_d = 1100 \pm 50$ W, as it was experimentally tested to be the most stable. A magnetic field topology correspondent to an electromagnet current strength of 1.5 A is selected (see Fig. 11 and Section 4.2). Notice that the discharge power obtained when running 2.0 mg/s is not the target ($P_d = 1100 \pm 50$ W) due to the low discharge voltage obtained in these measurements; therefore it is not included in Figs. 10(c), 10(d) nor 10(e).

From the results obtained, it can be seen that low mass flow rates, although generating less thrust (Fig. 10(c)), result in higher I_{sp} (Fig. 10(d)) which is ultimately reflected in higher efficiency (Fig. 10(e)). This performance could be an indication of a low propellant utilization: the thruster does not effectively use the extra mass flow provided when a higher water vapour flow is served. As discussed in Section 3, this could be due to the dissociation and ion dissociation reactions which water vapour undergo. The amount of energy used in these reactions supposes losses compare to single ionization events. In the past, the same mass flow trend was observed when testing with oxygen with this thruster [11]. Therefore, for both propellants, the lower the mass flow rate, the greater the thrust efficiency. Also, it can be seen how the TTPR is greater for the mass flow rate of 1.0 mg/s versus 2.0 mg/s. The TTPR seems to be pretty stable within the I_{sp} range investigated.

Plasma stability decreases when mass flow decreases, which prevented testing below mass flow rates of $\dot{m} = 0.7$ mg/s. Mass flow rates greater than $\dot{m} = 2.0$ mg/s ended in water condensation and could not be fully explored in full detail. However, some tests in this range suggested that the same trend of decreasing thrust efficiency can be expected, as in Fig. 10. In terms of stability and thrust performance, the most stable regime of the thruster is $\dot{m} = 1.0$ mg/s, conditions which will be kept for the rest of the experimentation.

4.2. Magnetic field dependence

Now that the preferable mass flow condition has been determined ($\dot{m} = 1.0$ mg/s), the thruster performance is tested under different magnetic field strengths. Fig. 11 compiles the results from these experiments in terms of voltage (Fig. 11(a)), TTPR versus I_{sp} (Fig. 11(b)), thrust (Fig. 11(c)), I_{sp} (Fig. 11(d)) and thrust efficiency (Fig. 11(e)). The performance plots are represented as a function of the peak magnetic field, according to Fig. 2, in the range of $B = 0.024 - 0.061$ T. Higher magnetic field strengths could not be tested because of the difficulties for the thruster to operate stably. This is because the resistance path of the electrons towards the anode increases as the magnetic field does. When the resistance is too high, the plasma is not

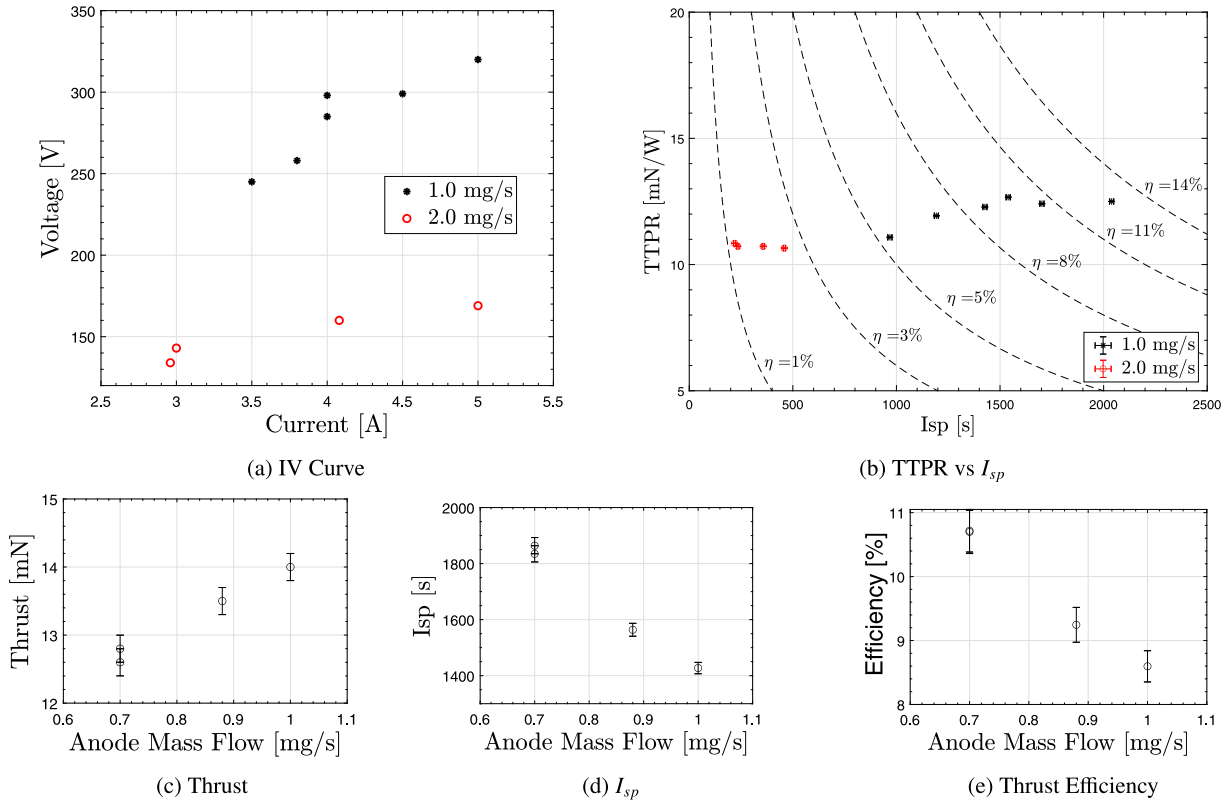

Fig. 10. Experimental measurements of a water vapour HET over different mass flow rates. Thrust, I_{sp} and thrust efficiency values are presented for a discharge power of $P_d = 1100 \pm 50$ W, a maximum magnetic field strength of 0.06 T (corresponding to an electromagnet current strength of 1.5 A, Fig. 11) and the geometrical configuration of Table 1.

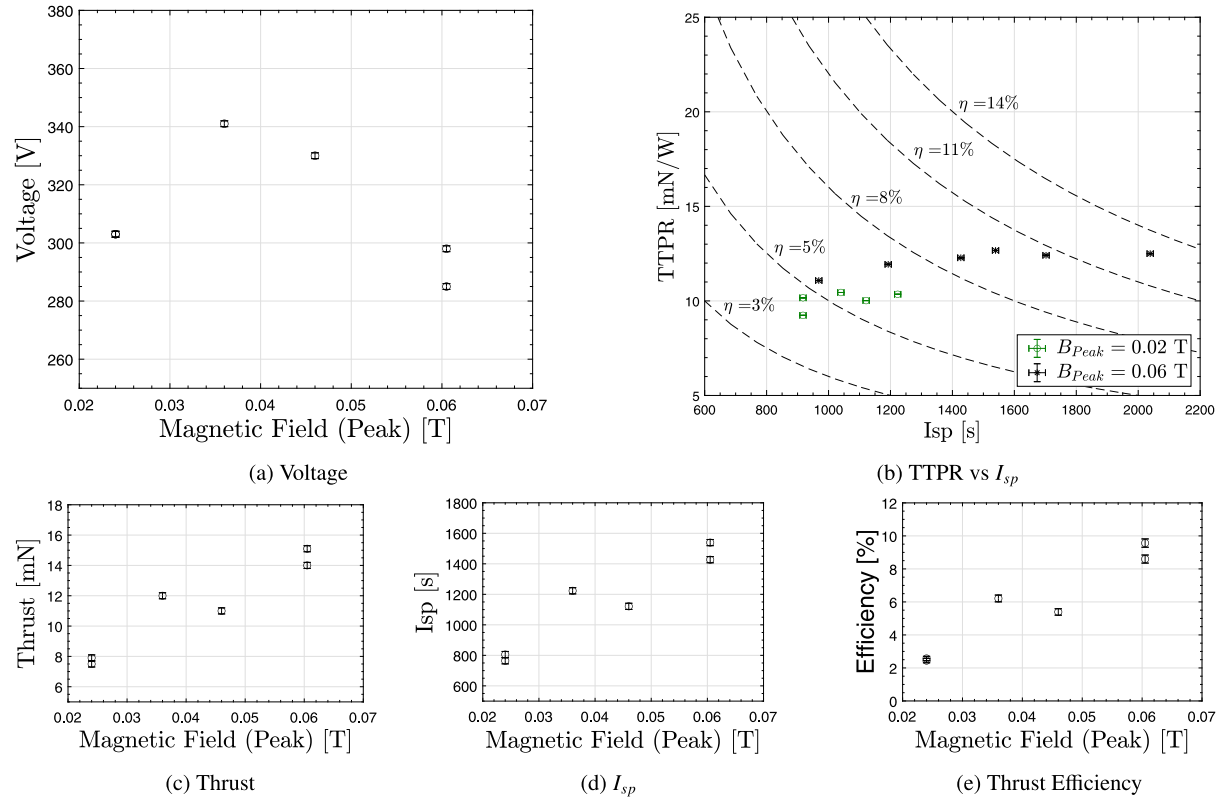

Fig. 11. Experimental measurements of a water vapour HET over a maximum magnetic field strength of $B = 0.024 - 0.061$ T, corresponding to the Gaussian magnetic topologies of Fig. 11. Values presented for a discharge power of $P_d = 1170 \pm 50$ W, mass flow $\dot{m} = 1.0$ mg/s and geometrical configuration of Table 1.

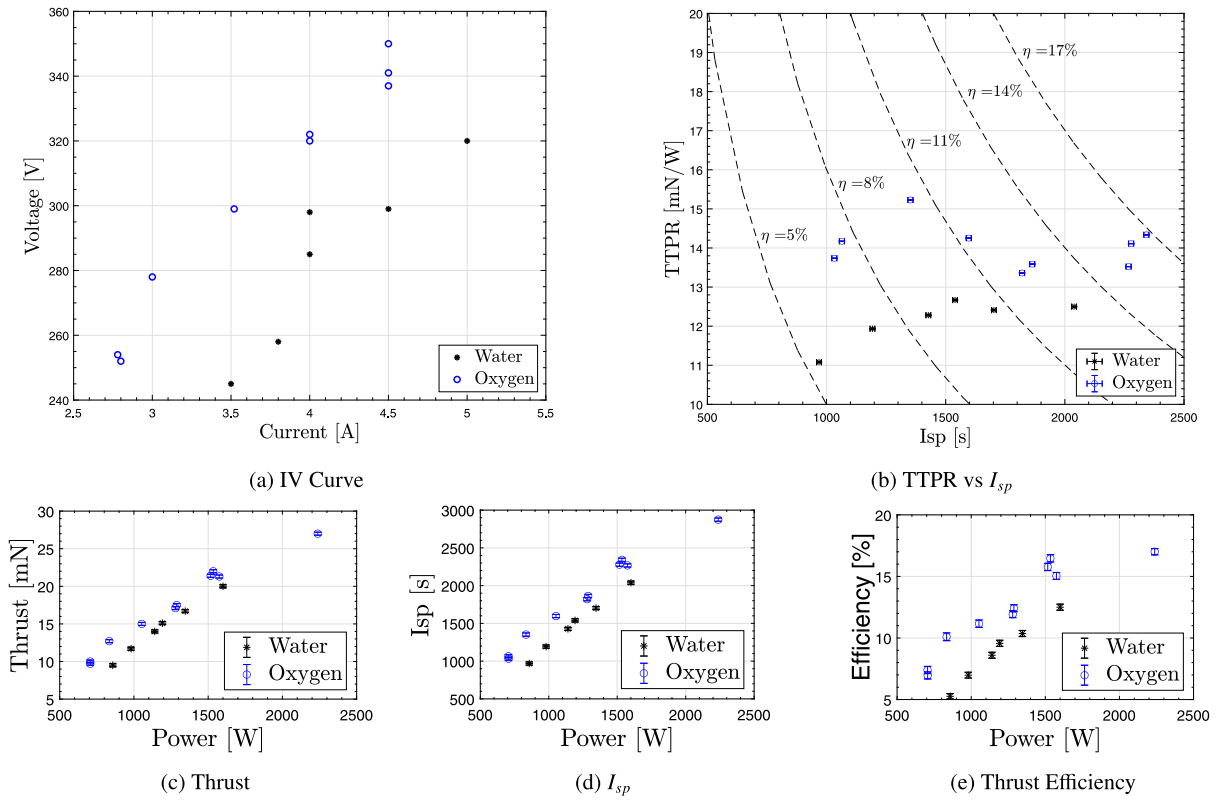

Fig. 12. Experimental measurements of a water vapour HET, for a discharge power range of $P_d = 600 - 1600$ W. Values presented for a mass flow of $\dot{m} = 1.0$ mg/s, peak magnetic field strength of 0.06 T (correspondent to an electromagnet current of 1.5 A, Fig. 11) and geometrical configuration of Table 1. Values compared with oxygen [14] under the same conditions.

sustained and, therefore, is extinguished. The discharge power used to compare these thrust measurements was $P_d = 1170 \pm 50$ W, similarly as in Section 4.1.

From the results obtained, it can be seen that, the higher the magnetic field strength, the higher the thrust (Fig. 11(c)), I_{sp} (Fig. 11(d)) and thrust efficiency (Fig. 11(e)). The maximum performance was obtained with a peak magnetic field strength of $B = 0.061$ T. Notice that this value is significantly larger than those typically used in standard xenon fuelled HETs. For comparison, the *SPT-100* uses a Gaussian magnetic field topology whose maximum strength peaks at $B = 0.016$ T [41] (almost 4 times weaker). In previous work with oxygen, a very similar behaviour was found [11,13] where these strong magnetic fields were preferential. In the TTPR representation, it can also be seen how higher I_{sp} and efficiencies are achieved when a stronger magnetic field is used.

4.3. Power range dependence

Fig. 12 shows the current intensity–voltage (IV) curve (Fig. 12(a)), TTPR versus I_{sp} (Fig. 12(b)), thrust (Fig. 12(c)), I_{sp} (Fig. 10(d)) and thrust efficiency (Fig. 12(e)) of the HET working with water vapour throughout the discharge power range of $P_d = 600 - 1600$ W. For these tests, the mass flow is set to 1.0 mg/s, since it is the most stable to operate the thruster with (Section 4.1). The magnetic field strength is set to the one correspondent to a peak value of $B = 0.061$ T (see Fig. 11 and Section 4.2).

The performance of the thruster operating with water vapour is now compared to that of oxygen (expected to be the result of a water electrolysis HET [14]), under the same magnetic field configuration and mass flow operating point; as resulted to be the most beneficial conditions in both cases. The main idea behind this comparison is to understand how these two propellants compare with each other when analysing them under the same conditions. This not only considers the same thruster geometrical and physical configuration and operating points, but also with the same cathode propellant (krypton). Only in this way, it is possible to have a direct comparison between these two gases that fuel the thruster without introducing other uncertainty sources which might affect this comparison. Notice, however, that in a flight-level system, the cathode propellant might be different in water vapour technology and water electrolysis. As remarked in Section 2.4, whereas the choice of cathode propellant for water electrolysis is clear (hydrogen), the best cathode propellant choice for water vapour yet needs to be further investigated (see Section 5). Although the cathode propellant is expected to have a non-substantial effect on the thruster operation (which is mainly governed by the thruster propellant), this point should still be noted when analysing these results.

From Fig. 12(a), it is appreciated that the discharge voltage of the thruster when operating with water vapour is lower than when working with oxygen. That could be an indication that the ionization rate of water vapour is lower compared to the one of oxygen, as discussed in Section 3. For both cases and throughout the entire power range of investigation, the voltage linearly keeps increasing as does the current. This behaviour would correspond to the "low voltage mode" of a HET working with xenon. For xenon however, it is experimentally seen that at a knee point (situated at a certain discharge current, 1.6 A in other studies [40]), the IV curve slope abruptly raises (enabling a "high voltage mode" of the thruster). This is something that is not appreciated either in water vapour or oxygen, where only one operating regime appears.

From the TTPR versus I_{sp} analysis (Fig. 12(b)), it is observed that TTPR remains pretty stable as a function of I_{sp}. However, there seems to be an indication of a sweep spot where the TTPR peaks, found on efficiencies of around $\eta = 11\%$, for both oxygen and water vapour.

Table 4
Comparison of the *WET-HET* running with lightweight propellants versus the *SPT-100*, running with xenon. The relative performance difference taking the *SPT-100* as a baseline is also shown.

	Propellant	Power [W]	Mass flow [mg/s]	Thrust [mN]	I_{sp} [s]	Anode efficiency [%]
SPT-100 [42.43]	Xenon	1520	4.93	87.6 (–)	1720 (–)	51.2% (–)
WET-HET	Water Vapour	1600 ± 1	1.00 ± 0.01	20.0 ± 0.2 (-77%)	2039 ± 20 (+19%)	12.5 ± 0.3 (-76%)
WET-HET	Oxygen	1534 ± 1	1.00 ± 0.01	22.0 ± 0.2 (-75%)	2243 ± 25 (+30%)	15.8 ± 0.3 (-69%)
WET-HET	Air	1525 ± 1	1.00 ± 0.01	21.3 ± 0.2 (-76%)	2267 ± 25 (+32%)	15.1 ± 0.3 (-70%)

Table 5
Representative Trade-off table between Water Vapour propulsion and Water Electrolysis HET propulsion.

	Factor weight	Water vapour (# Points)	Water electrolysis (# Points)	Description
Performance	High	Low	Medium	According to the research presented in this article, the performance of water electrolysis surpasses the one of water vapour for the investigated conditions. On average, water electrolysis is 20% more efficient considering the same geometrical configuration, cathode propellant and operating point.
Cathode Compatibility	High	Low	Medium	For water electrolysis, the selection of the propellant for the cathode is more straightforward: the electrolyzer separates water into oxygen (for the thruster) and hydrogen (for the cathode). Hydrogen is set to eliminate poisoning and is compatible with cathodes [26,27], although it still needs to be experimentally tested. For water vapour propulsion however, the right choice of propellant for the cathode remains an open question: a separate tank of krypton or xenon can be used to feed the cathode or a microwave cathode can be used to include water vapour [28], among others. This choice is part of the future investigation of this research.
Mass and Volume budget	Medium	Medium	High	Water vapour does not need an electrolyzer on board of the spacecraft, which lessens the amount of mass on board, overall cost and the technical difficulties of qualifying extra hardware. However, water electrolysis propulsion depends on the use of the electrolyzer and increases the mass and volume onboard.
Power budget	Medium	Low	Low	Water electrolysis needs heating systems to keep the electrolyzers under the operating temperature range (around 80 °C), and whose efficiency increases with the operating temperature. Water vapour propulsion also needs heating systems to keep the gas in vapour form. However, these amounts of power (≈50 W) are relatively low compared to the discharge power of the thruster (≈1500 W).

The thrust (Fig. 12(c)) linearly raises as the discharge power does, same for the I_{sp}. In both cases, water vapour does not perform as well as oxygen, which is something ultimately reflected in the thrust efficiency (Fig. 12(e)). Taking an average throughout all the discharge power, it is calculated that oxygen is roughly 20% more efficient than water vapour under the same testing conditions.

To put the performance of this thruster into perspective with other propellants, Table 4 shows the performance of the *WET-HET* with lightweight propellants against the *SPT-100* running with xenon.[1] The experimental results show how the *WET-HET* is able to provide a better I_{sp} in exchange of a considerably lower thrust. As expected, the performance of the thruster running with alternative propellants is considerably lower than with xenon. The *WET-HET* operating with air behaves very similarly as with oxygen, as seen in Table 4. However, the thruster is able to stably sustain the discharge at lower mass flow rates when using air, which increased the total performance (a similar trend as in the case of water, see Fig. 10). The best performance obtained was at a discharge power of $P_d = 1485$ W and mass flow rate of $\dot{m} = 0.9$ mg/s. This set point ended up in a performance corresponding to a thrust of 21.0 ± 0.2 mN, I_{sp} of 2433 ± 29 s and thrust efficiency of 16.9 ± 0.3%.

Fig. 13 also shows the propellant utilization efficiency of the *WET-HET* running with water vapour and oxygen, in comparison with the *SPT-100* running with xenon (data taken from the literature [13,21,22,42]). Notice that the propellant utilization efficiency does not come from direct measurements of the ion beam energy but from an

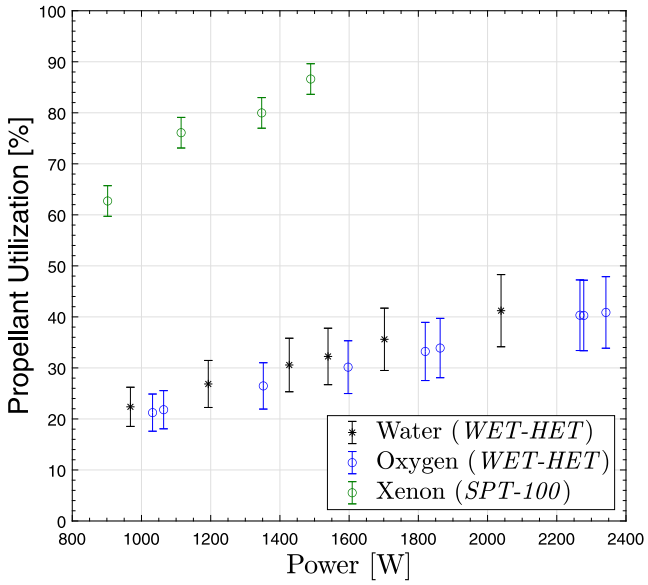

Fig. 13. Propellant utilization.

[1] The *WET-HET* is not taken as a comparison due to the fact that this thruster is solely optimized for lightweight propellants. Therefore, using this thruster as a reference to compare with heavy traditional propellants might not give a realistic comparison of the full potential of these thrusters operating with krypton and xenon.

analytical formulation computed as follows [13,42]:

$$\alpha = \frac{I_i}{I_{\dot{m}}} = \frac{T}{\dot{m}\sqrt{V_d(1-\delta)2e/m_n}} \tag{4}$$

where I_i is the ion current, $I_{\dot{m}} = e\dot{m}/m_n$ is equivalent current for the injected mass flow for the elementary charge e and neutral mass m_n and δ is a parameter related to the discharge efficiency which typically varies from 0.1–0.3 [43]. Being conservative, the coefficient δ is supposed to vary between $0 < \delta < 0.5$ [13]. Hence, the error bars are calculated by either taking $\delta = 0$ (lower error bar) or $\delta = 0.5$ (upper error bar). As expected, the propellant utilization efficiency for xenon thrusters like the *SPT-100* is greater than any other HET working with alternative propellants. Due to the uncertainty in the parameter δ, and due to the fact that this is an analytical calculation, it is not possible to assess whether if water vapour or oxygen has a higher propellant utilization. However, it gives an indication about the percentage loss and the comparison with the state-of-the-art HETs.

Finally, in some measurements when experimenting with water vapour, an "anomalous" mode of operation was found, characterized by a substantially lower discharge voltage ($V_d < 200$ V). Under these conditions, the performance of the thruster was poor, with efficiency levels lower than 6% which, did not increase with power, but rather remained flat throughout the discharge power investigated ($P_d = 600-1600$ W). It is believed that this mode is triggered when the heating power of the plasma filament cathode is excessive. This extra heating creates an electron release which makes the plume of the thruster and the cathode to merge together, and then the thruster actuates in this lower impedance mode with poor performance. By decreasing the power of the cathode heating, this phenomenon was avoided.

Now that the performance of these technologies has been shown, a system level analysis comparing water vapour and oxygen is addressed hereafter.

5. Trade off between water electrolysis and water vapour fuelled HETs

The previous sections have shown how the performance of water vapour changes under different mass flows, magnetic field strengths and discharge powers. These data were compared with oxygen data in the same testing scenario (see Section 4.3). From these results, oxygen (from water electrolysis) is roughly 20% more efficient than water vapour in HETs. However, the trade-off between water vapour and water electrolysis is not just limited to the performance of the thruster. The cathode compatibility and mass, volume and power budgets need to be addressed to get the full picture of how these technologies compare to each other.

Table 5 compares water vapour and water electrolysis HET propulsion using the lessons learnt from the last years of experimentation and the results obtained in this paper. A qualitative estimation is presented. There, water vapour and water electrolysis are compared for each category selected: performance [1], cathode compatibility [2], mass and volume budget [3] and power budget [4]. This comparison shows some of the advantages and disadvantages of these technologies. In terms of performance and cathode compatibility (factors chosen as the most important ones), water electrolysis outweighs water vapour. The contrary happens when looking at the mass and volume budgets. There, water vapour HETs are preferred due to the independence from a water electrolyser to function. Powerwise, these two system require little extra power to work, compared to the amount needed for a standard HET to run. Note that these two technologies are still evolving, and future results can modify the discussion shown in Table 5. To further exploration would be the assessment of the possible contamination of the satellite when in contact with water vapour, whose condensation might create ice around some critical components when being in space.

6. Conclusions and future work

In this work, a HET operating with water vapour is investigated. A bespoke water feed system is used to allow for a liquid-vapour phase change and to fuel the thruster. A liquid mass flow meter sets the operating point, and, downstream, a capillary tube is used to increase the fluidic resistance of water and create a sudden expansion at the end of the tube; which ultimately causes the evaporation of water. A heating system is used to raise the temperature of the pipelines and prevent water condensation. By means of a pressure transducer, the pressure of the line is monitored to determine if water condensation has occurred. Following an analysis of the pipe losses using the Darcy-Weisbach equation, the total length of the line was reduced and the diameter of the pipe thickened, reducing pressure losses throughout the line from the thruster exit to the flow restrictor. After these iterations on the water feedline, mass flows below 2 mg/s could be used without condensation. As the nominal operating point of the thruster is 1 mg/s, this set-up permits the experimentation with no restrictions. By taking pressure measurements at the flow restrictor and computing the pressure surges coming from the Darcy–Weisbach equation, the pressure levels throughout the line are estimated. The location of highest pressure within the feedline is found at the thruster injection point, due to the small gaps used to transport the propellant to the discharge channel.

The experimental campaigns have investigated the HET under the mass flow range of 0.7–1.0 mg/s. From these results, it is observed that although by using a lower mass flow the thrust is reduced, the thrust efficiency is higher. For stability reasons however, a mass flow of 1.0 mg/s is preferable. Experimental results in this operating point have analysed the performance of the thruster under different magnetic fields strengths in the range 0.024–0.061 T. A Gaussian magnetic field topology peaking at 0.061 T is the most beneficial one in terms of thrust efficiency. Higher magnetic fields strengths could not be tested due to the high resistance of the electrons in the magnetized zone, which ultimately destabilizes and extinguishes the plasma. With that magnetic field topology, the thruster performance was measured in the discharge power range of $P_d = 600$–1600 W and compared with oxygen.

By looking at the reactive model of these two molecules, a poorer performance for water vapour was predicted. This was thought to be because, in the case of water vapour, the cross-section of the OH dissociative reaction ($H_2O + e \rightarrow OH + H + e$) is higher than any ionization process. The energy used when dissociating the molecule does not contribute to the thrust as it does not generate ions, and therefore, it is an energy loss in the system. In the case of oxygen, the opposite situation is found: for most of the electron energies, the ionizing reaction O_2^+ is more statistically more probable than the dissociating one. The experiments conducted with both propellants under the same thruster and operating conditions ratified this prediction, showing the oxygen is approximately 20% more efficient than water vapour. On the basis of these results, a representative trade-off analysis between water vapour and water electrolysis propulsion is conducted. Performance, cathode compatibility, mass, volume and power budgets are the factors selected to make this comparison. The mass and volume budgets of water vapour are less than those with water electrolysis, merely because of the lack of an electrolyzer onboard of the spacecraft. In terms of the power requirements, although both technologies need extra power to accommodate a heating system and/or an electrolyzer, these requirements are not significant compared to the discharge power of the thruster. All in all, the type of space mission and its requirements will ultimately decide which propulsion technology is the most favourable.

In future work, it is expected to characterize the plume of the HET operating with these propellants using an E × B probe and perform experiments with a hydrogen cathode (for water electrolysis). A revised version of the HET will be characterized and tested using the lessons learnt from this experimentation.

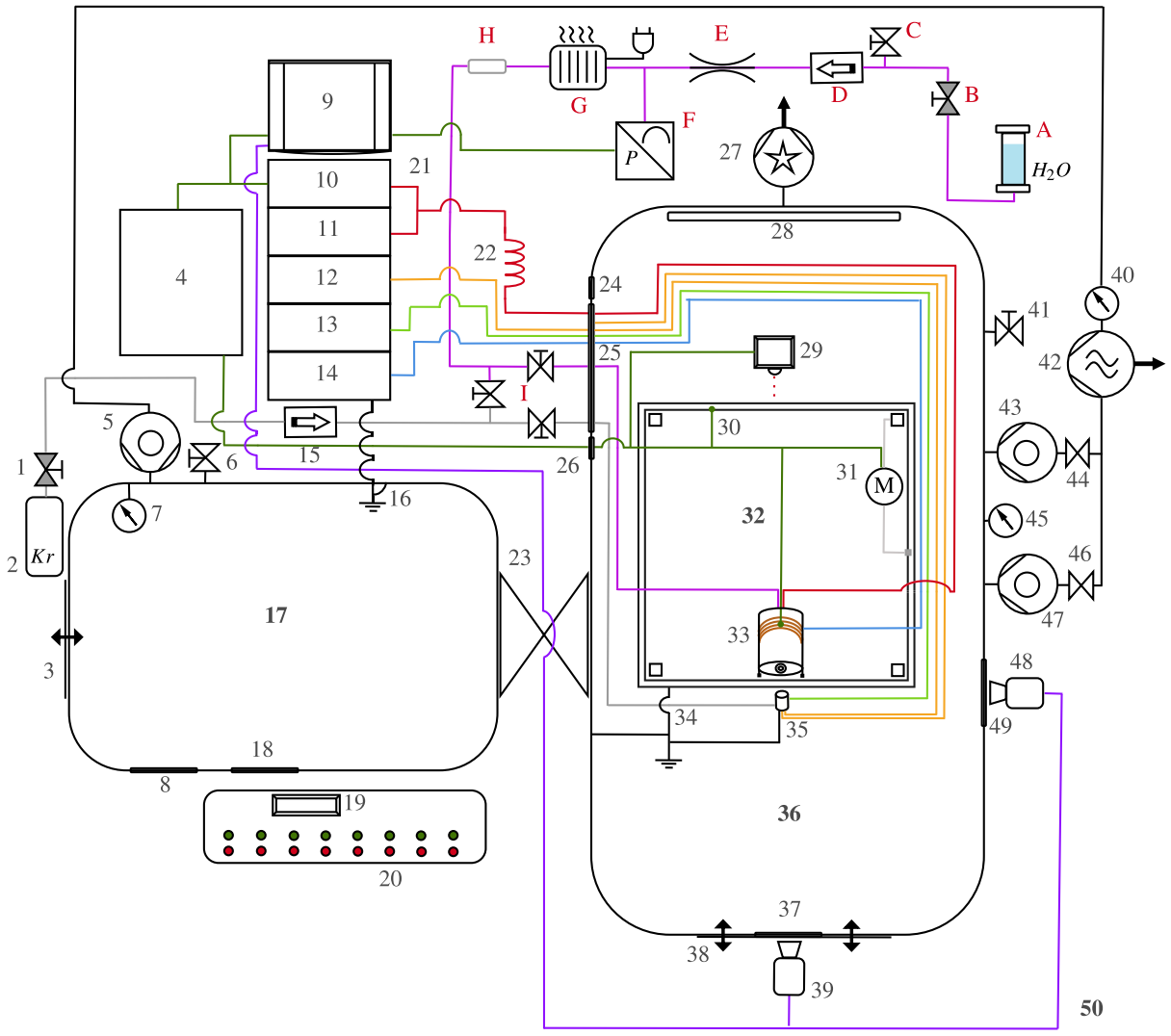

Fig. A.14. Main schematics of the Water Vapour Electric Space Propulsion testing at the Imperial Plasma Propulsion Laboratory, IPPL (Department of Aeronautics, Imperial College London).

Table A.6
Description of the elements depicted in Fig. A.14.

1	Pressure regulator (cathode)
2	Cathode propellant bottle (Krypton)
3	Door (vacuum load-lock hatch chamber)
4	Electronics box
5	Turbopump (load-lock hatch chamber)
6	De-pressurizing valve (load-lock hatch chamber)
7	Pressure gauge (to load-lock hatch chamber)
8	Vacuum feedthrough (auxiliary)
9	Computer station
10	Anode power supply [master] (*Sorenson SGA 1K0X5S-0AA*)
11	Anode power supply [slave] (*Sorenson SGA 1K0X5S-0AA R*)
12	Heater power supply (*Electro-Automatik EA-PSI 8080-60 DT*)
13	Keeper power supply (*Glassman PS/ET05R400-200*)
14	Magnet power supply (*GW INSTEK SPS-3610*)
15	Mass flow controller (cathode)
16	Grounding connection
17	Vacuum load-lock hatch chamber
18	Vacuum feedthrough (window)
19	Pressure readings display
20	Control panel of vacuum systems
21	Parallelizing line (anode power supplies)

(*continued on next page*)

Table A.6 (*continued*).

22	Inductor
23	Gate valve
24	Vacuum feedthrough (auxiliary)
25	Vacuum feedthrough (power and feedlines)
26	Vacuum feedthrough (signals, D-Sub connector)
27	Cryohead (connected to a cryocompressor)
28	Cryohead (connected to a cryocompressor)
29	Laser ILD1750
30	Thermocouple (to thrust balance)
31	Servomotor (for calibration)
32	Thrust balance
33	Water Electrolysis HET
34	Grounding connection
35	Cathode (double filament)
36	Main vacuum chamber
37	Vacuum feedthrough (window)
38	Door (main vacuum chamber)
39	Camera Nikon D-5000 (front)
40	Pressure gauge (to roughing pump)
41	De-pressurizing valve (main chamber)
42	Roughing pump (Stage 1)

(*continued on next page*)

Table A.6 (*continued*).

43	Turbopump #1 (Stage 2, Leybold)
44	Pneumatic valve #1
45	Pressure gauge (to main chamber)
46	Pneumatic valve #2
47	Turbopump #2 (Stage 2, Leybold)
48	Camera Nikon D-5000 (side)
49	Vacuum feedthrough (window)
50	Imperial College London Plasma Laboratory

Declaration of competing interest

The authors declare that they have no known competing financial interests or personal relationships that could have appeared to influence the work reported in this paper.

Acknowledgements

The authors would like to acknowledge the support of the European Space Agency, The Netherlands in the development of the research. Likewise, we would also like to acknowledge the support of *URA Thrusters* and *ALIENA Pte Ltd*, who intensively collaborate with the research presented throughout the article.

Funding

This research is developed together with the European Space Agency in a co-funded PhD programme under the reference ESA RFP/3-17304/21/NL/GLC/my.

Appendix. Main schematics of the EP testing

The following diagram (Fig. A.14) shows the complete set of hardware, electronics and fluidics used for the experimentation. The description of the elements depicted in Fig. A.14 is listed in Table A.6. More information about the set-up can be found in previous work [14].

References

[1] D.M. Goebel, I. Katz, Fundamentals of Electric Propulsion, John Wiley & Sons, Ltd, 2008, pp. 325–392.
[2] J. del Amo, Activities on electric propulsion at ESA, in: 37th International Electric Propulsion Conference, IEPC-2022-346, Massachusetts Institute of Technology, Cambridge, MA, USA, 2022.
[3] D. Lev, et al., The technological and commercial expansion of electric propulsion, Acta Astronaut. 159 (2019) 213–227, http://dx.doi.org/10.1016/j.actaastro.2019.03.058.
[4] A. Hepp, B. Palaszewski, A. Colozza, G. Landis, D. Jaworske, M. Kulis, In-situ resource utilization for space exploration: Resource processing, mission-enabling technologies, and lessons for sustainability on earth and beyond, in: 12th International Energy Conversion Engineering Conference, IECEC 2014, 2014, http://dx.doi.org/10.2514/6.2014-3761.
[5] J.M. Tejeda, A. Schwertheim, A. Knoll, Water as an environmentally friendly propellant for a multi-functional spacecraft architecture, International Journal of Energetic Materials and Chemical Propulsion 22(2) (2023) 21–33, http://dx.doi.org/10.1615/IntJEnergeticMaterialsChemProp.v22.i2.20.
[6] M.W. Crofton, T.D. Hain, Environmental considerations for xenon electric propulsion, in: 30th International Electric Propulsion Conference, 2007.
[7] M.Y. Savinov, A.M. Arkharov, V.E. Poznyak, V.L. Bondarenko, Development and creation of an efficient Khrom-3 unit for preparing krypton-xenon mixtures, Chem. Petrol. Eng. 43 (2007) 259–269, http://dx.doi.org/10.1007/s10556-007-0047-3.
[8] United Kingdom (UK) Government, Department for Business, Energy & Industrial Strategy, Government GHG conversion factors for company reporting: Methodology paper for emission factors: final report, 2018.
[9] M. Swiatek, Capturing and recycling of xenon from a cryopumped vacuum chamber, in: 46th AIAA/ASME/SAE/ASEE Joint Propulsion Conference &Amp; Exhibit, http://dx.doi.org/10.2514/6.2010-6798.
[10] J.B. Bovill, Inhalation anaesthesia: from diethyl ether to xenon, Mod. Anesth. (2008) 121–142.
[11] A. Schwertheim, A. Knoll, Low power thrust measurements of the water electrolysis hall effect thruster, CEAS Space J. 14 (2022) 3–17, http://dx.doi.org/10.1007/s12567-021-00350-y.
[12] J.M. Tejeda, A. Knoll, A water electrolysis hall effect thruster computational model with radiofrequency excitation, in: 37th International Electric Propulsion Conference, IEPC-2022-313, Massachusetts Institute of Technology, Cambridge, MA, USA, 2022.
[13] A. Schwertheim, A. Knoll, Experimental investigation of a water electrolysis hall effect thruster, Acta Astronaut. 193 (2022) 607–618, http://dx.doi.org/10.1016/j.actaastro.2021.11.002.
[14] J.M. Tejeda, A. Knoll, An oxygen-fuelled hall effect thruster: Channel length, ceramic walls and anode material experimental analyses, Acta Astronaut. 203 (2023) 268–279, http://dx.doi.org/10.1016/j.actaastro.2022.11.055.
[15] A. Faust, Adriane, R.J. Sedwick, Performance of a helicon thruster using helium, argon, and water vapor, in: 52nd Aerospace Sciences Meeting, 2014, p. 0141.
[16] D. Staab, et al., Aquajet: an electrodeless ECR water thruster, in: Space Propulsion Conference, 2018.
[17] R. Moloney, et al., Experimental validation and performance measurements of an ECR thruster operating on multiple propellants, in: 36th International Electric Propulsion Conference, IEPC-2019-199, University of Vienna, Vienna, Austria, 2019.
[18] Y. Nakagawa, H. Koizumi, Y. Naito, K. Komurasaki, Water and xenon ECR ion thruster—comparison in global model and experiment, Plasma Sources. Sci. Technol. 29 (10) (2020) 105003.
[19] J. Asakawa, H. Koizumi, K. Yaginuma, K.Y. Nakagawa, Yuichi, Pre-flight testing results of multiple water propulsion systems-resistojet and ion thruster for SmallSats, in: Small Satellite Conference, Utah State University, United States, 2022.
[20] A. Schwertheim, A. Knoll, The water electrolysis hall effect thruster (WET-HET): Paving the way to dual mode chemical-electric water propulsion, in: 36th International Electric Propulsion Conference, IEPC-2019-A259, University of Vienna, Vienna, Austria, 2019.
[21] J.M. Sankovic, J.A. Hamley, T.W. Haag, Performance evaluation of the Russian SPT-100 thruster at NASA LeRC, NASA STI/Recon Technical Report N, 1994, p. 23630.
[22] J.R. Brophy, Stationary plasma thruster evaluation in Russia. Provided by the SAO/NASA astrophysics data system, 1992, Provided By the SAO/NASA Astrophysics Data System.
[23] A. Schwertheim, et al., Interlaboratory validation of a hanging pendulum thrust balance for electric propulsion testing, Rev. Sci. Instrum. 92 (3) (2021) 034502, http://dx.doi.org/10.1063/5.0037100.
[24] B. Wolf, Handbook of Ion Sources, CRC Press, 1995, http://dx.doi.org/10.1201/9781315214054.
[25] J. Polk, The effect of reactive gases on hollow cathode operation, in: 42nd AIAA/ASME/SAE/ASEE Joint Propulsion Conference & Exhibit, 2006, p. 5153.
[26] H.E. Gallagher, Poisoning of LaB6 cathodes, J. Appl. Phys. 40 (1) (1969) 44–51, http://dx.doi.org/10.1063/1.1657092.
[27] D.M. Goebel, J.T. Crow, A.T. Forrester, Lanthanum hexaboride hollow cathode for dense plasma production, Rev. Sci. Instrum. 49 (4) (1978) 469–472, http://dx.doi.org/10.1063/1.1135436.
[28] T. Motoki, D. Takasaki, H. Koizumi, Y. Ataka, K. Komurasaki, Y. Takao, Experimental study on the performance characteristics of a miniature microwave discharge cathode, Acta Astronaut. 196 (2022) 231–237.
[29] Darwin Microfluidics, Microfluidic flow resistance kit, 2022, https://darwin-microfluidics.com/. (Online Accessed 10 October 2022).
[30] I.H. Bell, S. Quoilin, J. Wronski, V. Lemort, Coolprop: An open-source reference-quality thermophysical property library, in: ASME ORC 2nd International Seminar on ORC Power Systems, sn, 2013, p. 181.
[31] R.A. Chilton, S. Richard, Pressure loss equations for laminar and turbulent non-Newtonian pipe flow, J. Hydraulic Eng. 124 (5) (1998) http://dx.doi.org/10.1061/(ASCE)0733-9429(1998)124:5(522).
[32] G.O. Brown, The history of the Darcy-weisbach equation for pipe flow resistance, Environ. Water Resou. History 38 (7) (2002) 34–43.
[33] T.L. Bergman, A.S. Lavine, F.P. Incropera, D.P. DeWitt, Fundamentals of Heat and Mass Transfer, Seventh ed., John Wiley & Sons, Inc., 2011.
[34] Y. Itikawa, N. Mason, Cross sections for electron collisions with water molecules.
[35] Y. Itikawa, Cross sections for electron collisions with oxygen molecules, J. Phys. Chem. Ref. Data 38 (1) (2009) 1–20, http://dx.doi.org/10.1063/1.3025886.
[36] A. Li, R. Nussinov, A set of van der waals and coulombic radii of protein atoms for molecular and solvent-accessible surface calculation, packing evaluation, and docking, Proteins: Struct. Function and Bioinform. 32 (1) (1998) 111–127.
[37] S.S. Batsanov, Van der waals radii of elements, Inorg. Mater. 37 (9) (2001) 871–885.
[38] J.M. Tejeda, M. Reza, F. Faraji, A. Knoll, Performance enhancement of hall effect thrusters using radiofrequency excitation, Acta Astronaut. 194 (2022) 145–161, http://dx.doi.org/10.1016/j.actaastro.2022.01.033.
[39] J.M. Haas, Low Perturbation Interrogation of the Internal and Near-Field Plasma Structure of a Hall Thruster using a High-Speed Probe Positioning System, University of Michigan, 2001.

[40] T. Nakagawa, N. Yamamoto, K. Komurasaki, Y. Arakawa, Experimental investigation of a hall thruster using oxygen as the propellant, Japan Soc. Aeronaut. Space Sci. 51 (598) (2003) 606–612.
[41] I. Mikellides, I. Katz, M. Mandell, J. Snyder, A 1-D model of the hall-effect thruster with an exhaust region, in: 37th Joint Propulsion Conference and Exhibit, 2001, http://dx.doi.org/10.2514/6.2001-3505.
[42] K. Dannenmayer, S. Mazouffre, Elementary scaling relations for hall effect thrusters, J. Propuls. Power 27 (2011) 236–245, http://dx.doi.org/10.2514/1.48382.
[43] T. Ito, N. Gascon, Nicolas, W. Crawford, M. Cappelli, Experimental characterization of a micro-hall thruster, J. Propuls. Power 23 (5) (2007) 1068–1074, http://dx.doi.org/10.2514/1.27140.